Langmuir

Article

pubs.acs.org/Langmuir

Thermocapillary-Driven Motion of a Sessile Drop: Effect of Non-Monotonic Dependence of Surface Tension on Temperature

George Karapetsas,*[,†] Kirti Chandra Sahu,[‡] Khellil Sefiane,[∥] and Omar K. Matar[§]

[†]Department of Mechanical Engineering, University of Thessaly, Volos 38334, Greece

[‡]Department of Chemical Engineering, Indian Institute of Technology Hyderabad, Yeddumailaram 502 205, Andhra Pradesh, India

[∥]School of Engineering, University of Edinburgh, Faraday Building, Mayfield Road, Edinburgh, EH9 3JL, United Kingdom

[§]Department of Chemical Engineering, Imperial College London, London SW7 2AZ, United Kingdom

ABSTRACT: We study the thermocapillary-driven spreading of a droplet on a nonuniformly heated substrate for fluids associated with a non-monotonic dependence of the surface tension on temperature. We use lubrication theory to derive an evolution equation for the interface that accounts for capillarity and thermocapillarity. The contact line singularity is relieved by using a slip model and a Cox-Voinov relation; the latter features equilibrium contact angles that vary depending on the substrate wettability, which, in turn, is linked to the local temperature. We simulate the spreading of droplets of fluids whose surface tension−temperature curves exhibit a turning point. For cases wherein these turning points correspond to minima, and when these minima are located within the droplet, then thermocapillary stresses drive rapid spreading away from the minima. This gives rise to a significant acceleration of the spreading whose characteristics resemble those associated with the "superspreading" of droplets on hydrophobic substrates. No such behavior is observed for cases in which the turning point corresponds to a surface tension maximum.

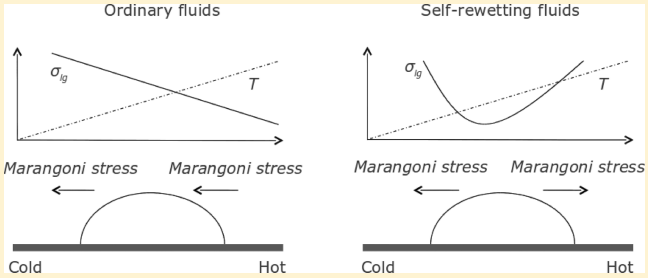

INTRODUCTION

The motion of sessile droplets over liquids and solids is of central importance to a number of industrial applications such as coating flow technology, inkjet printing, microfluidics and microelectronics, and medical diagnostics. Despite the apparent simplicity of the physical setup involved, this motion is rather complex and some of its aspects remain poorly understood; in particular, the mechanisms underlying the dynamics of the three-phase contact line are still the subject of debate. In view of its complexity[1] and its practical importance, droplet motion has received considerable attention in the literature and has been the subject of two major reviews.[2,3]

In this work, we consider the motion of sessile droplets on non-isothermal solid walls, driven by thermocapillarity. The walls underlying the droplets are subjected to a temperature gradient which induces surface tension gradient-driven droplet deformation and migration from low to high surface tension regions. Thermocapillary-driven droplet motion was studied by Bouasse[4] who demonstrated the possibility of inducing droplet-climbing on a heated wire, against the action of gravity, by heating its lower end. Studies involving horizontal substrates have shown that, unless the magnitude of the imposed temperature gradient is sufficiently large, no droplet motion is possible due to contact angle hysteresis, while under certain conditions, steady migration of droplets has been shown.[5,6]

A number of studies have examined the thermocapillary motion of droplets theoretically. Brochard[7] determined the spreading characteristics of a wedge-shaped drop in the presence of chemical or thermal gradients via local force and energy balances. This work was generalized by Ford and Nadim[8] to arbitrary, two-dimensional droplet shapes and different contact angles at the two contact lines. Lubrication theory was used to describe the spreading of a droplet on a uniformly heated wall,[9,10] and Anderson and Davis[11] accounted for evaporative effects. These effects were also considered by Karapetsas et al.[12] who showed that the flow is accompanied by the formation of hydrothermal waves. Thermocapillary nonwetting was studied by Chen et al.,[13] while buoyancy-driven convection was also examined by Nguyen et al.[14]

Quasi-steady solutions of the lubrication equations in the presence of thermal gradients were determined by Smith[15] to correspond to two states: a motionless drop, or a steadily migrating drop, deformed toward the cooler region of the substrate. More recently, Gomba and Homsy[16] relieved the contact line singularity with a precursor model and solved the lubrication equations with the contact angle varying parameterically. Their results showed that spreading is accompanied by ridge-formation at the contact line for small contact angles, while for large contact angles, drop translation with fixed shape was observed. These authors also demonstrated the existence of a regime at intermediate values of the contact angle characterized by drop breakup.

Received: January 21, 2014
Revised: March 25, 2014
Published: April 2, 2014

   dx.doi.org/10.1021/la5002682 | *Langmuir* 2014, 30, 4310−4321

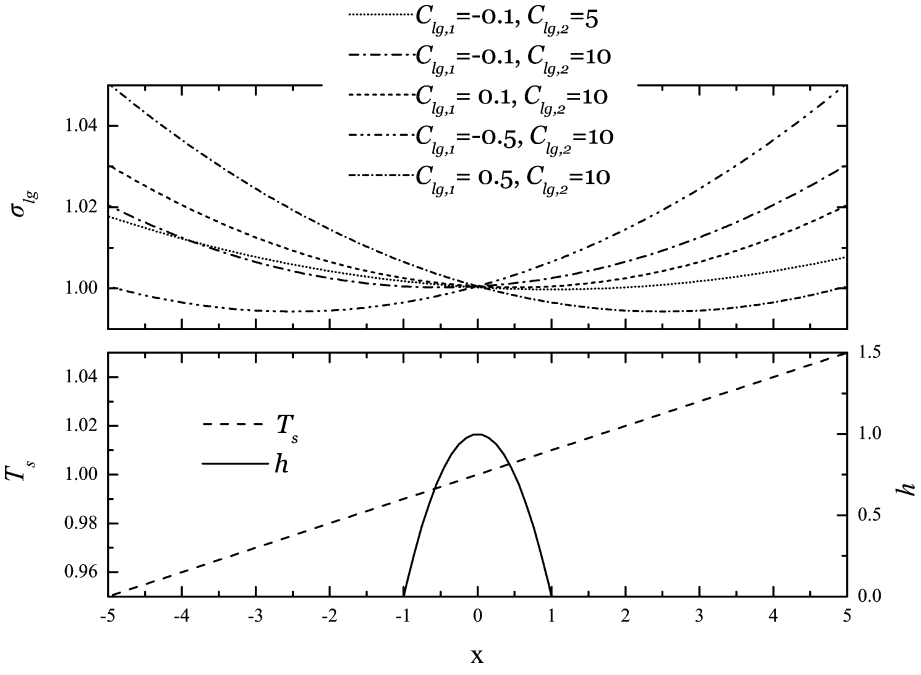

Figure 1. Variation of temperature and the gas−liquid surface tension, σ_{lg}, in the x-direction for different $C_{lg,1}$ and $C_{lg,2}$ values, and with $\Gamma = 0.01$. The h profile is given by eq 22.

The contact angle depends on temperature through its dependence on the vapor−liquid, liquid−solid, and vapor−solid surface tensions. The work of Pratap et al.,[17] who performed experiments using decane drops on polydimethylsiloxane (PDMS)-coated substrates, has demonstrated this fact clearly through the significant departure of the contact line from a circular shape and the variable droplet migration velocity; the latter was shown to decrease with increasing proximity to the colder substrate regions. Although Pratap et al.[17] have ascribed their observations to the reduction in droplet size due to evaporation and an increase in its viscosity due to substrate cooling, they did not consider local variations in the wettability to play a role. This is surprising since wettability gradients have been shown experimentally to drive rapid droplet motion efficiently[18,19] via the imposition of substrate temperature gradients.

The work on droplet migration in the presence of thermal gradients described in the foregoing review[16−19] elucidates the importance of the contact angle on the dynamics and its dependence on temperature. The theoretical work of Gomba and Homsy,[16] however, considers a constant contact angle. This was realized by Karapetsas et al.[20] who accounted for temperature-induced varying substrate wettability which allowed them to incorporate dynamically varying contact angles in their lubrication equations. This, in turn, permitted them to study the delicate interplay between contact line dynamics and thermocapillarity on non-isothermal substrates. Their results demonstrate that the droplet motion is accompanied by complex dynamics which includes enhanced spreading rates, non-monotonic dependence of the contact line speed on the applied substrate temperature gradient, and "stick−slip"-type behavior.

In the present paper, we extend the work of Karapetsas et al.[20] to fluids that have a non-monotonic dependence of the surface tension on temperature. In particular, these so-called "self-rewetting" fluids,[21−26] which are non-azeotropic, high carbon alcohol solutions, have parabolic surface tension−temperature curves with well-defined minima; the parabolicity of these curves increases with alcohol concentration. These fluids were first studied by Vochten and Petre[21] who observed the occurrence of the minimum in surface tension with temperature in high carbon alcohol solutions. Petre and Azouni[22] carried out experiments that involved imposing a temperature gradient on the surface of alcohol aqueous solutions, and used talc particles to demonstrate the unusual behavior of these fluids. The nonlinear thermocapillary effect on thin liquid films was studied by Oron and Rosenau[27] and later by Slavtchev and Miladinova.[28] Experimental work on these fluids was also carried out under reduced-gravity condtions.[24] The term "self-rewetting" was coined by Abe et al.[29] who studied the thermophysical properties of dilute aqueous solution of high carbon alcohols. Due to thermocapillary stresses, and the shape of the surface tension−temperature curve, the fluids studied spread "self-rewet" by spreading spontaneously towards the hot regions, thereby preventing dry-out of hot surfaces and enhancing the rate of heat transfer. Due to these properties, "self-rewetting" fluids were shown to be associated with substantially higher critical heat fluxes compared to water.[30−32] Savino et al.[25] illustrated the anomalous behaviour of self-rewetting fluids by performing experiments to visualize the behaviour of vapour slugs inside wickless heat pipes made of pyrex borosilicate glass capillaries. They found that the size of the slugs was considerably smaller than that associated with fluids such as water. More recently, work on self-rewetting fluids was extended to microgravity conditions for space applications on the International Space Station,[26] and Hu et al.[33] demonstrated that the use of these fluids within micro oscillating heat pipes led to an increase in the efficiency of these devices.

We consider constant substrate temperature gradients and use lubrication theory to derive a single evolution equation for the interface dynamics, in the high-conduction limit, in which the contact angle varies locally with temperature. Our results indicate that for self-rewetting fluids, the spreading rate far exceeds that of fluids with a monotonic surface tension dependence on temperature. This spreading is characterized by power-law exponents that approach unity, and is punctuated by the formation of pronounced capillary ridges at the contact line.

dx.doi.org/10.1021/la5002682 | Langmuir 2014, 30, 4310−4321

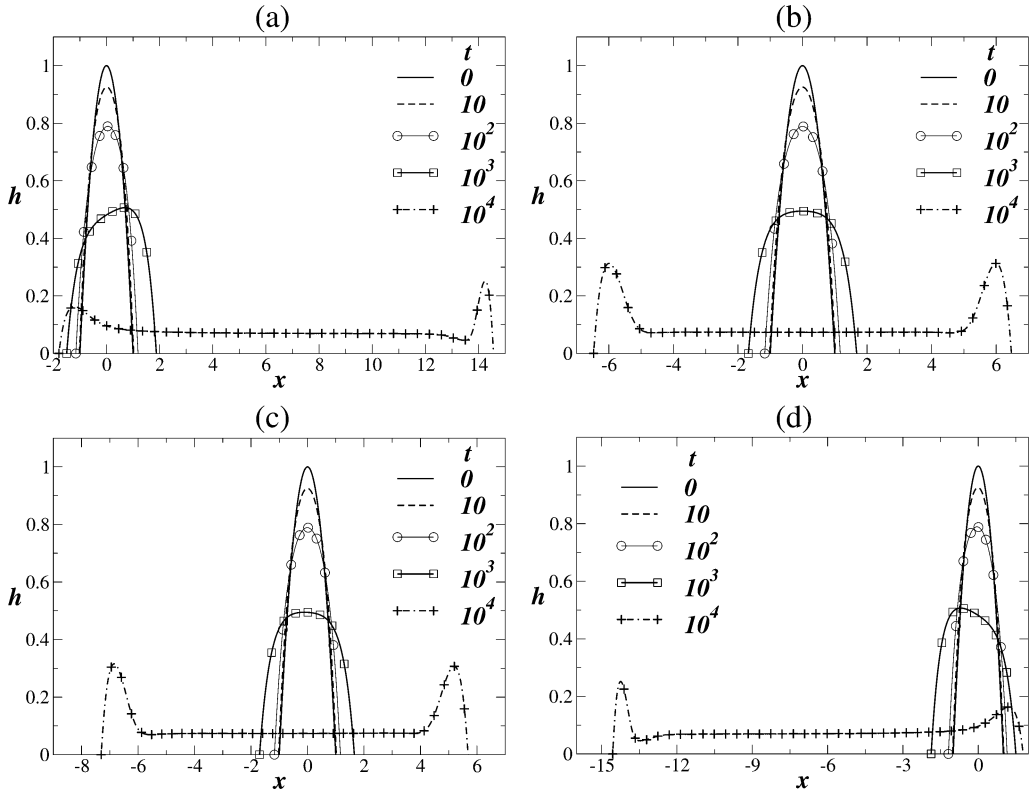

Figure 2. Evolution of the drop profile for $\theta_{a,l} = \theta_{a,r} = 0.447$ and for (a) $C_{lg,1} = -0.1$, (b) $C_{lg,1} = 0$, (c) $C_{lg,1} = 0.01$, and (d) $C_{lg,1} = 0.1$. The rest of the parameter values are $\varepsilon = 0.1$, Ca = 100, $C_{lg,2} = 10$, $k = 10^{-3}$, $m = 3$, Bo = 0.5, $\Gamma = 0.01$, $\delta_{ls} = 1$, and $S = -0.001$. The locations of the minimum surface tension in panels (a), (b), (c), and (d) are −0.5, 0, 0.05, and 0.5, respectively.

These features are reminiscent of droplets undergoing "superspreading",[34] which has been observed to be previously driven by the addition of certain surfactant molecules, or the application of electric fields.[35]

The rest of the paper is organized as follows. In Section II, we outline the main steps of the derivation of the evolution equation for the interface dynamics, and the numerical method used for its numerical solution; full details of this derivation are provided by Karapetsas et al.[20] The results are presented and discussed in Section III. Finally, the concluding remarks are given in Section IV.

PROBLEM FORMULATION

We study the motion of a two-dimensional drop of an incompressible, Newtonian fluid on a horizontal, rigid, and impermeable solid wall. The fluid has a constant density ρ, viscosity μ, specific heat capacity C_p, and thermal conductivity λ. The temperature-dependent surface tensions of the liquid−gas, liquid−solid, and solid−gas interfaces are σ_{lg}, σ_{ls}, and σ_{sg}, respectively. The drop maximal thickness and half-width are given by H and L, and we assume that $H/L \ll 1$, which permits the use of lubrication theory. We note that this theory assumes small slopes and therefore cannot be used to model droplet spreading at high contact angles (usually exceeding 30−40°[36,37]). A Cartesian coordinate system, (x,z), is used to describe the flow in which x and z denote the horizontal and vertical coordinates, respectively, with the wall located at $z = 0$ and the gas−liquid interface at $z = h(x,t)$. The two-dimensional velocity field is $\mathbf{u} = (u,w)$ where u and w denote the horizontal and vertical velocity components, respectively. The distribution of the temperature, T, along the wall is given by $T_w = T_o + \gamma x$ in which T_w denotes the temperature of the wall and T_o is the wall temperature at $x = 0$, while $\gamma \equiv dT_w/dx$ is a constant.

The equations of mass, momentum, and energy conservation govern the flow dynamics. Solutions of these equations are obtained subject to a tangential and normal stress balance, as well as a kinematic boundary condition imposed at $z = h(x,t)$. We assume the rate of heat transfer from the interface to be negligible and set the thermal flux to zero at $z = h(x,t)$; this is supported by the fact that, for typical experimental conditions, the Biot number is small.[5,6,38] We also impose continuity of temperature at $z = 0$. In addition, at the liquid−solid interface, we apply the no-penetration condition on w, and a Navier slip condition on u[39] to relieve the stress singularity which would otherwise arise at the moving contact line: $u = \beta u_z$; here, β is a slip length. A nonlinear constitutive relation for the dependence of the interfacial tensions on temperature is chosen to model the behavior of a self-rewetting fluid:

$$\sigma_i = \sigma_{i,o} + \frac{d\sigma_i}{dT}\Big|_{T_o}(T_s - T_o) + \frac{1}{2}\frac{d^2\sigma_i}{dT^2}(T_s - T_o)^2 \quad (i = lg, ls, sg) \tag{1}$$

where T_s is the temperature at the corresponding interface, and $\sigma_{i,o}$, $(i = lg, ls, sg)$ denotes the surface tension of all interfaces at the reference temperature, T_o.

We choose the following scalings in order to render the governing equations and boundary conditions dimensionless:

dx.doi.org/10.1021/la5002682 | Langmuir 2014, 30, 4310−4321

$$(x, z, h) = L(\tilde{x}, \varepsilon\tilde{z}, \varepsilon\tilde{h}) \quad t = \frac{L}{U}\tilde{t} \quad (u, w) = U(\tilde{u}, \varepsilon\tilde{w})$$

$$p = \frac{\mu UL}{H^2}\tilde{p} \quad T = \tilde{T}T_o \quad \sigma_i = \sigma_{lg,o}\tilde{\sigma}_i \quad (i = lg, ls, sg) \tag{2}$$

The tilde symbol that designates the dimensionless variables is suppressed henceforth. Here, p denotes the pressure, t represents time, and $U = \varepsilon\sigma_{lg,o}/\mu$ is a characteristic velocity; $\mathrm{Ca} = \mu U/\varepsilon^3\sigma_{lg,o}$, $\mathrm{Bo} = \rho g H^2/\mu U$, $\Gamma = \gamma L/T_o$, and $B = \beta/H$ correspond to the capillary and Bond numbers, and a dimensionless thermal gradient and slip length, respectively. Substitution of these scalings into the governing equations and boundary conditions yields the following set of equations using the lubrication approximation:

$$u_x + w_z = 0 \tag{3}$$

$$p_x = u_{zz} \quad p_z = -\varepsilon Bo \tag{4}$$

$$T_{zz} = 0 \tag{5}$$

$$z = h(x, t): \quad h_t + u|_h h_x = w|_h \quad p|_h = -Ca^{-1}\sigma_{lg}h_{xx}$$
$$u_z|_h = \sigma_{lg,x} \quad T_z|_h = 0 \tag{6}$$

$$z = 0: \quad u = Bu_z \quad w = 0 \quad T_w = 1 + \Gamma x \tag{7}$$

The detailed derivation of these equations is given in Karapetsas et al.[20] Solution of eqs 3−5, and use of the boundary conditions 6 and 7, yields

$$T = T_w \tag{8}$$

and the following evolution equation for h

$$h_t = \left[\left(\frac{h^3}{3} + Bh^2\right)p_x - \sigma_{lg,x}\left(Bh + \frac{h^2}{2C_{lg}}\right)\right]_x \tag{9}$$

where the pressure gradient, p_x, is given by

$$p_x = -\mathrm{Ca}^{-1}(\sigma_{lg}h_{xx})_x + \varepsilon \mathrm{Bo} h_x \tag{10}$$

and the dimensionless form of the constitutive equation for the surface tension is given by

$$\sigma_{lg} = 1 - C_{lg,1}(T_s - 1) + C_{lg,2}(T_s - 1)^2 \tag{11}$$

$$\sigma_i = \delta_i[1 - C_{i,1}(T_w - 1) + C_{i,2}(T_w - 1)^2] \qquad (i = ls, sg) \tag{12}$$

in which $C_{i,1} = -(\mathrm{d}\sigma_i/\mathrm{d}T)(T_o/\sigma_{i,o})$, $C_{i,2} = 1/2(\mathrm{d}^2\sigma_i/\mathrm{d}T^2)(T_o^2/\sigma_{i,o})$, and $\delta_i = (\sigma_{i,o}/\sigma_{ig,o})$, $(i = lg, ls, sg)$. It follows from eq 8 that the interfacial temperature is $T_s = T|_h = T_w$ given by

$$T_s = T_w = 1 + \Gamma x \tag{13}$$

Using eqs 11, 12, and 13, it is possible to determine the position of maximum/minimum surface tension by using the following expression

$$x_m = -\frac{C_{i,1}}{2C_{i,2}\Gamma} \tag{14}$$

At the contact line, we set the interface height to zero

$$h(x = x_{cl}, t) = h(x = x_{cr}, t) = 0 \tag{15}$$

where x_{cl} and x_{cr} denote the location of the left and right contact lines, respectively. We use an empirical constitutive equation for the dependence of the contact line speed on the contact angle,[40] which has been employed by numerous researchers previously to study contact line motion.[11,34,41−44] The dimensionless form of this relation, in the absence of contact angle hysteresis, is given by the Cox-Voinov-Tanner law

$$\frac{\mathrm{d}x_{cl}}{\mathrm{d}t} = -k_l(\theta_l - \theta_{a,l})^m$$
$$\frac{\mathrm{d}x_{cr}}{\mathrm{d}t} = k_r(\theta_r - \theta_{a,r})^m \tag{16}$$

where θ_l and θ_r are the dynamic contact angles at x_{cl} and x_{cr}, respectively, and $\theta_{a,j}$, $(j = l,r)$ are the corresponding advancing contact angles, taken to be equal to the equilibrium contact angle, which may vary depending on the wall temperature local to the position of the corresponding contact line. In eq 16, k_j are mobility exponents (here, we will assume that $k_l = k_r = k$), and m will take values in the range $1 \le m \le 3$. Other forms of a similar power law dependence have been suggested in the literature based on local analysis near the contact line, i.e., $\mathrm{d}x_{ci}/\mathrm{d}t \approx \theta_i^3 - \theta_{a,i}^3$,[45] which, however, give qualitatively similar predictions. As noted by Karapetsas et al.,[20] imposing the Navier slip condition away from the contact line, and the Cox-Voinov relation at the contact line, is similar to using a generalized Navier boundary,[46] which relates the contact line speed to a viscous stress contribution, and an extra contribution due to an uncompensated Young stress; the latter is present in out-of-equilibrium situations such as the one considered in the present work and exceeds greatly the viscous stress contribution at the contact line.

The equilibrium balance between the tangential interfacial forces at the contact line yields

$$\cos(\theta_{a,j}) = \frac{\sigma_{sg}(x_{cj}) - \sigma_{ls}(x_{cj})}{\sigma_{lg}(x_{cj})} \tag{17}$$

We set $\theta_{a,j} \to \varepsilon\theta_{a,j}$ in the lubrication approximation and, since $\cos(\varepsilon\theta) \sim 1 - \varepsilon^2\theta^2/2$ for $\varepsilon \ll 1$, we can deduce that

$$\theta_{a,j}^2 = -\frac{2}{\varepsilon^2}\frac{\sigma_{sg}(x_{cj}) - \sigma_{ls}(x_{cj}) - \sigma_{lg}(x_{cj})}{\sigma_{lg}(x_{cj})} \tag{18}$$

This expression for $\theta_{a,j}$ is used in eq 16 to represent the local influence of wall temperature on the contact line speed. If the right-hand-side of eq 18 becomes negative, we assume that the substrate is wetted perfectly and set $\theta_{a,j} = 0$. If the surface tensions of the substrates and liquids have an identical dependence on temperature, then $C_{lg,1} = C_{sg,1} = C_{ls,1}$ and $C_{lg,2} = C_{sg,2} = C_{ls,2}$, and the expression for the equilibrium contact angle reduces to

$$\theta_{a,j}^2 = -\frac{2}{\varepsilon^2}S \tag{19}$$

where $S = \delta_{sg} - \delta_{ls} - 1$ denotes the spreading parameter; S is kept small in order to be consistent with the lubrication approximation. Thus, only in this unlikely case does the advancing contact angle remain equal to the equilibrium contact angle at the reference temperature and independent of the position of the contact line.[20]

We map the transient physical domain, (x,t), onto a computational domain fixed in time, (x',t'), using

dx.doi.org/10.1021/la5002682 | Langmuir 2014, 30, 4310−4321

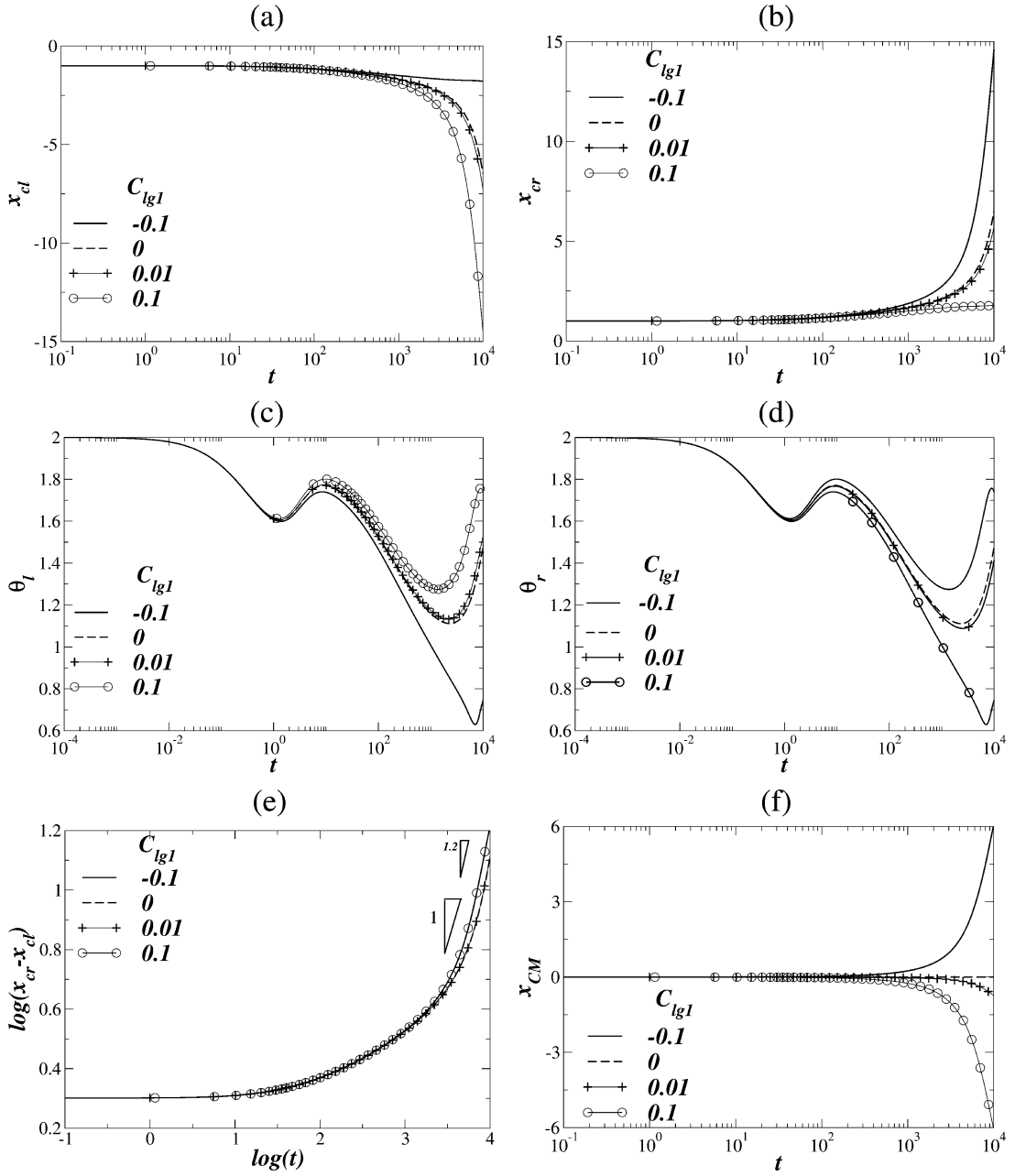

Figure 3. The position of the (a) left and (b) right contact lines of the drop versus time. Evolution of dynamic contact angles (c) θ_l, (d) θ_r for different values of $C_{lg,1}$. Evolution of (e) the extent of spreading, and (f) the position of the center of mass of the droplet for different values of $C_{lg,1}$. The rest of the parameter values are the same as those used to generate Figure 2.

$$x' = (x - x_{cl})\frac{x_{cr}(t=0) - x_{cl}(t=0)}{x_{cr} - x_{cl}} \tag{20}$$

so that the interior of the drop is mapped to $0 \le x' \le 1$, and the time-derivatives are expressed as follows:

$$\partial_t = \partial_{t'} - \frac{\mathrm{d}x'}{\mathrm{d}t}\partial_{x'} \tag{21}$$

The evolution equation for h is then solved numerically using a finite element/Galerkin method (details of the numerical procedure are given in refs 20,34) starting from the following initial conditions:

$$h(x,\, t=0) = 1 - x^2 \tag{22}$$

$$x_{cl}(t=0) = -1 \tag{23}$$

$$x_{cr}(t=0) = 1 \tag{24}$$

200 elements were used to discretize the computational domain in space, and the implicit Euler method was employed to advance the solution in time. The Newton−Raphson method was used to solve the resulting set of nonlinear algebraic equations at each time-step. Convergence was achieved upon mesh-refinement, and mass conservation was satisfied to within 1%. A discussion of the results is presented next.

RESULTS AND DISCUSSION

We begin the presentation of our results by showing in Figure 1 the variation of the surface tension, σ_{lg}, the interface height, h, and

dx.doi.org/10.1021/la5002682 | Langmuir 2014, 30, 4310−4321

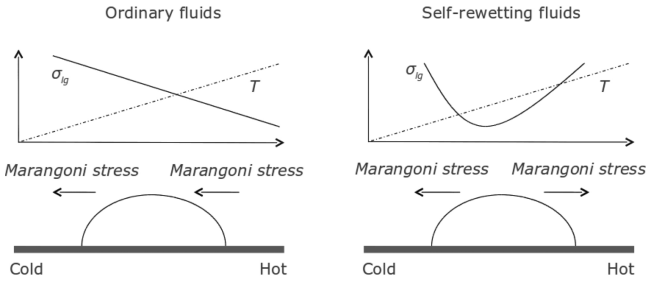

Figure 4. Schematic for the mechanism of the thermally enhanced spreading of self-rewetting fluids.

the temperature at the interface, T_s, with the horizontal coordinate, x. This variation is depicted for parameterically varying values of $C_{lg,1}$ and $C_{lg,2}$, the constants that control the linear and quadratic dependence of σ_{lg} on T_s, as dictated by eq 11. As is illustrated in Figure 1, the depth and location of the minimum of the σ_{lg}–x curve can be controlled by varying these parameters. Below, we discuss the spreading dynamics that are associated with starting from different locations of the minimum in relation to the initial position of the droplet. Numerical solutions were obtained over a wide range of parameter values. For typical applications $\Gamma \approx 10^{-4}$–0.02 and Bo $\approx 10^{-2}$–2. For the remainder of this paper we choose a representative "base" case and set $\varepsilon = 0.1$, Ca = 100, $k = 10^{-3}$, $m = 3$, Bo = 0.5, $\delta_{ls} = 1$, and $S = 0.001$. This set of parameters corresponds to the spreading of slender centimeter-size droplets.

Constant θ_a. To set the base of the discussion that follows we begin our study by considering the case of constant θ_a. This assumption is often enountered in the literature reflecting the independence of the equilibrium contact angle on the substrate wettability in response to local temperature variations. We assume that the equilibrium contact angle remains equal at all times to the equilibrium contact angle at the reference temperature (given by eq 19); for the particular values of ε and S, we have $\theta_{a,l} = \theta_{a,r} = 0.447$.

In Figure 2a, we show the spreading dynamics associated with the $C_{lg,1} = -0.1$ and $C_{lg,2} = 10$ case in which the σ_{lg}–x minimum lies initially to the left of the flow origin, $x = 0$, the symmetry plane for h. As can be seen in this panel, the droplet deforms in the direction of increasing surface tension driven by thermocapillarity. The spreading is highly asymmetric, reflecting the initial difference between the plane of symmetry of the drop and the initial location of the σ_{lg}–x minimum. Toward the latter stages of the spreading, a pronounced ridge is formed at the droplet right contact line, x_{cr}, in the direction of fastest spreading. In contrast, the location of the left contact line, x_{cl}, advances very little in the negative x direction. This is because the difference in σ_{lg} between the minimal σ_{lg} value and that at the left edge of the droplet is smaller than the corresponding difference associated with the right contact line. This is also reflected in Figure 3a and b in which we plot the temporal location of x_{cl} and x_{cr} and their dependence on $C_{lg,1}$.

We also track the temporal variation of the dynamic contact angles at the two contact lines, θ_l and θ_r, in panels (c)–(d) of Figure 3. As can be seen clearly in this figure, both contact angles decrease from their initial values, and exhibit oscillatory behavior at intermediate times. For the $C_{lg,1} = -0.1$ case, however, θ_l (θ_r) decreases (increases) at late times, which coincides with the

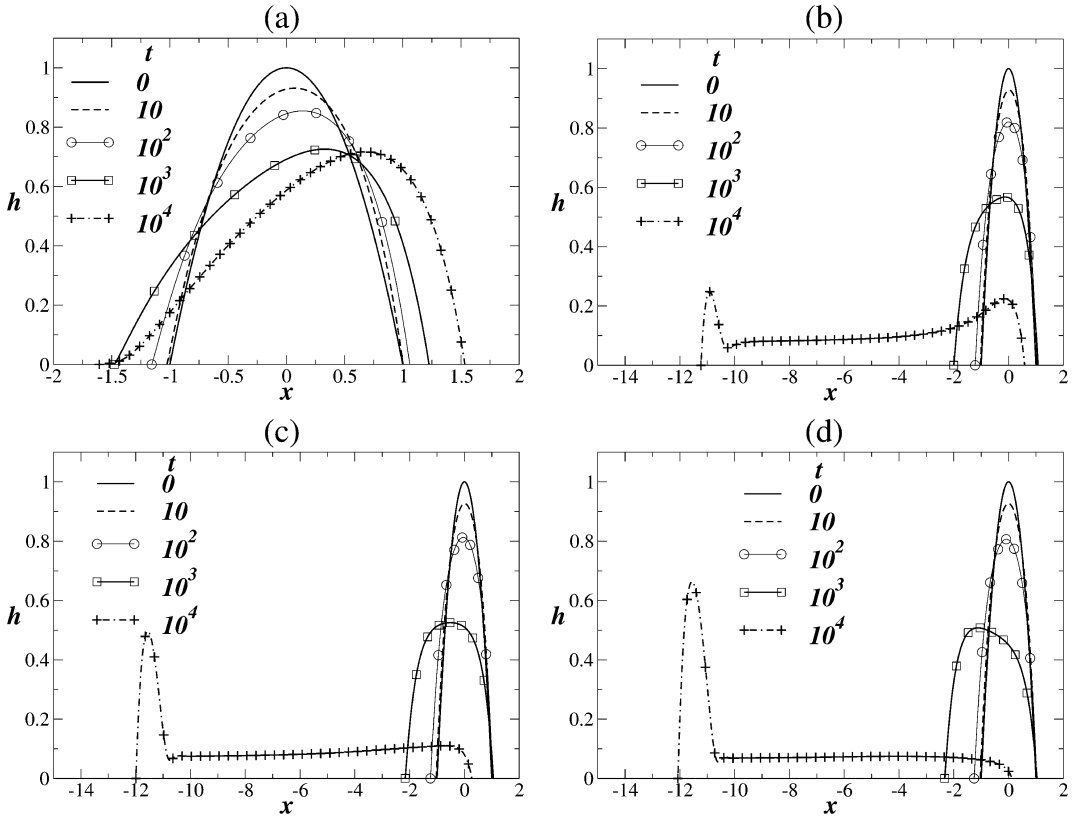

Figure 5. Evolution of the drop profile for (a) $C_{lg,1} = -0.5$, (b) $C_{lg,1} = -0.1$, (c) $C_{lg,1} = 0$, and (d) $C_{lg,1} = 0.1$. The rest of the parameter values are $\varepsilon = 0.1$, Ca = 100, $C_{ls1} = C_{sg1} = 1$, $C_{lg,2} = 10$, $C_{sg2} = C_{ls2} = 0$, $k = 10^{-3}$, $m = 3$, Bo = 0.5, $\Gamma = 0.01$, $\delta_{ls} = 1$, and $S = -0.001$. The locations of the minimum surface tension in panels (a), (b), (c), and (d) are −2.5, −0.5, 0, and 0.5, respectively.

dx.doi.org/10.1021/la5002682 | Langmuir 2014, 30, 4310–4321

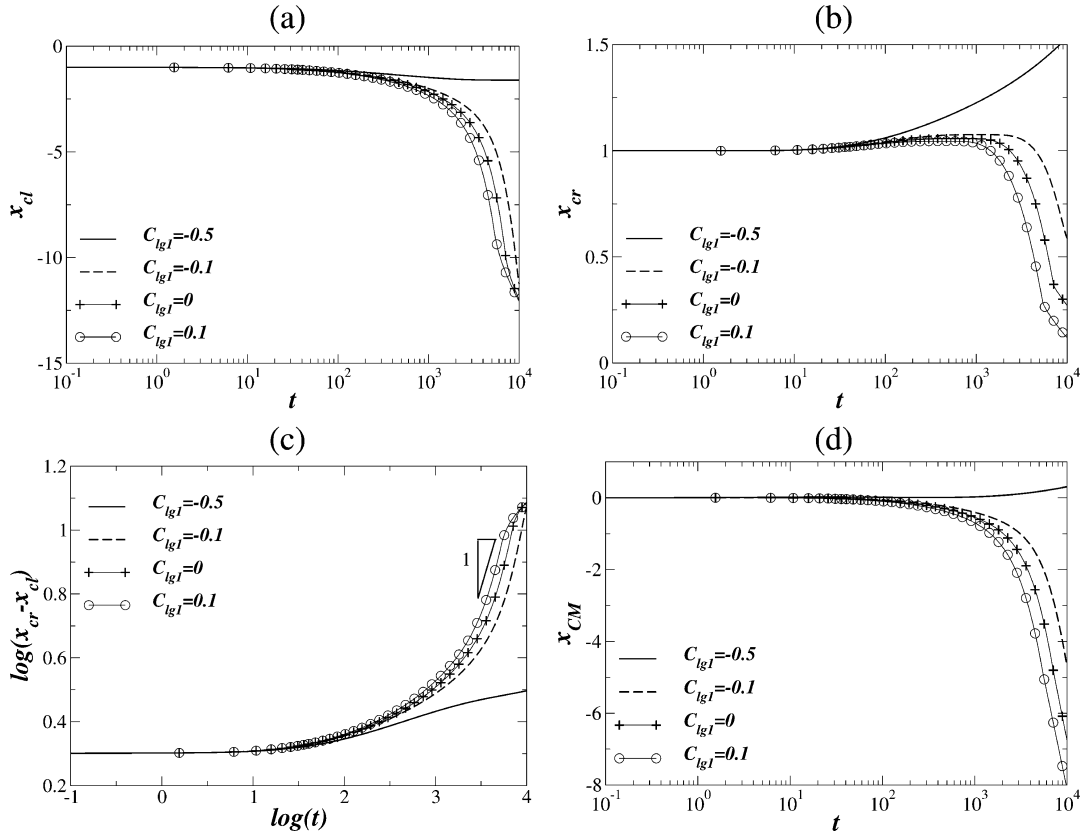

Figure 6. Position of the (a) left and (b) right contact lines of the drop versus time; evolution of the (c) extent of spreading; (d) position of the center of mass of the droplet for different values of $C_{lg,1}$. The rest of the parameter values are the same as those used to generate Figure 5.

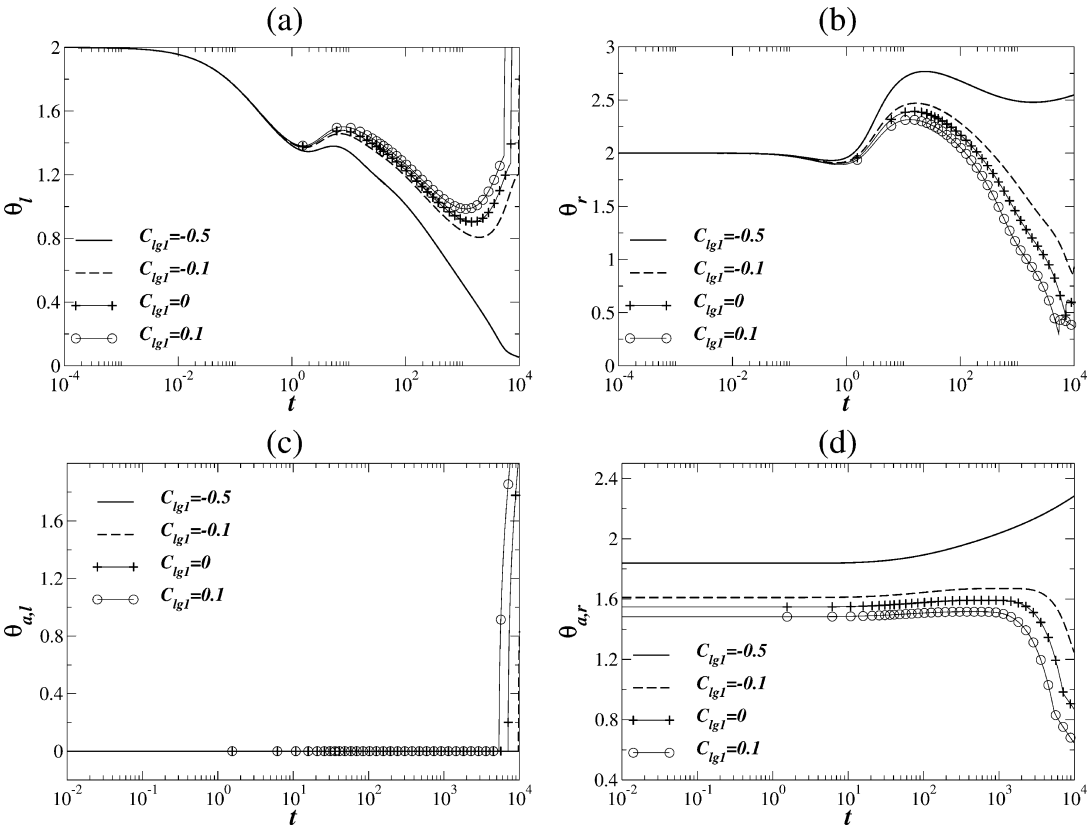

Figure 7. Evolution of dynamic contact angles (a) θ_l, (b) θ_r, and equilibrium contact angles (c) $\theta_{a,l}$ (d) $\theta_{a,r}$ for different values of $C_{lg,1}$. The rest of the parameter values are the same as those used to generate Figure 5.

dx.doi.org/10.1021/la5002682 | *Langmuir* 2014, 30, 4310−4321

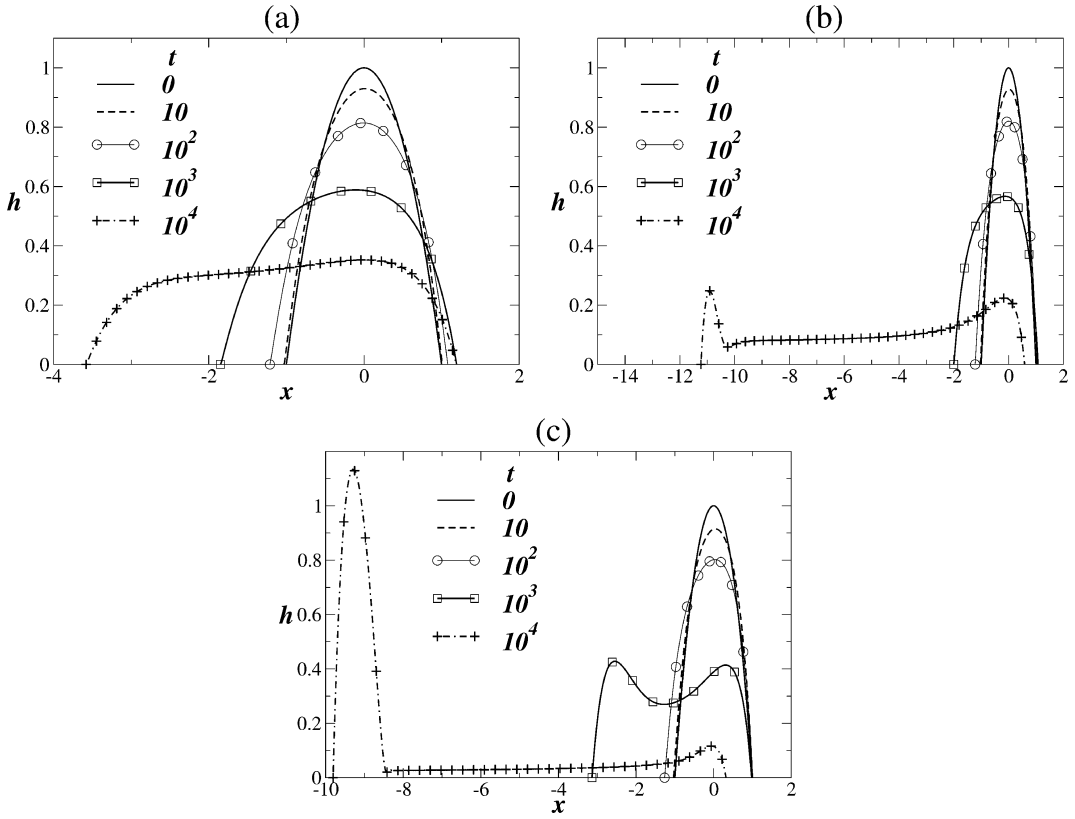

Figure 8. Evolution of the drop profile for (a) $\Gamma = 0.005$, (b) $\Gamma = 0.01$, and (c) $\Gamma = 0.02$. The rest of the parameter values are $\varepsilon = 0.1$, Ca = 100, $C_{ls1} = C_{sg1} = 1$, $C_{lg,1} = -0.1$, $C_{lg,2} = 10$, $C_{sg2} = C_{ls2} = 0$, $k = 10^{-3}$, $m = 3$, Bo = 0.5, $\Gamma = 0.01$, $\delta_{ls} = 1$, and $S = -0.001$. The locations of the minimum surface tension in panels (a), (b), and (c) are −1, −0.5, and −0.25, respectively.

formation of the pronounced ridge at x_{cr}. The temporal variation of the extent of spreading, measured by the difference in the location of the left and right contact lines, $x_{cr} - x_{cl}$, is also tracked and shown along with that of the droplet center of mass in panels (e) and (f) of Figure 3, respectively. It can be seen that the spreading exhibits power-law like behavior at sufficiently long times, characterized by large exponents; we estimate the latter to be between 1 and 1.2 during the latter stages of the spreading, as shown in panel (e). This result is striking since such large values of the spreading exponent have been observed in cases of droplets undergoing "superspreading" driven by the addition of certain surfactant molecules[34] or the application of electric fields.[35]

We also examine the effect that the difference between the locations of the σ_{lg}–x minimum and the drop symmetry plane exerts on the spreading dynamics. This is varied by altering the value of $C_{lg,1}$ while keeping all other parameters fixed. For $C_{lg,1} = 0$ the σ_{lg}–x minimum and symmetry plane are co-located, and as can be seen in Figure 2, the spreading is perfectly symmetric. For increasingly positive values of $C_{lg,1}$, the minimial σ value is located progressively to the right of the symmetry plane so that σ_{lg} is higher at the left boundary than it is on the right one. This then leads to thermocapillary-driven spreading from the minimal σ region toward higher σ_{lg} domains. Since the largest gradients are associated with the left boundary, spreading is fastest in that direction, as can be seen in panel (d) of Figure 2; this is a mirror image of the case presented in panel (a) of this figure. In all cases considered, thickened ridges are formed at the contact line advancing with the largest speed, and these are also associated with high power-law exponents, and the largest dynamic contact angles, as shown in Figure 3.

At this point, it is interesting to examine the mechanism that drives the enhanced spreading, as is shown in Figures 2–3. In the case of a fluid with a linear dependence of the surface tension on temperature, the Marangoni stresses always drive flow from hot to cold regions, acting in the same direction for both ends of the droplet (see Figure 4). On the other hand, in the case of a self-rewetting fluid, the dependence of surface tension on temperature is non-monotonic, which has a significant effect on the induced Marangoni stresses. When the position of minimum surface tension happens to be inside the droplet, the Marangoni stresses induce flow away from this position, in the direction of increasing tension located at the droplet edges. As a result, Marangoni stresses cause the latter to move in opposite directions, thereby stretching the droplet and enhancing the spreading rate.

As was implied above, the spreading of self-rewetting fluids shares some common characteristics with the "superspreading" that takes place in the presence of certain surfactants. To make this connection clearer, it is useful to mention two of the main characteristics of "superspreading" that have been observed experimentally: (a) very fast spreading with spreading exponents close to 1, and (b) the formation of ridge in the periphery of the drop. It appears that both these features are also present in the case of self-rewetting fluids (see Figures 2, 3). Karapetsas et al.[34] suggested that the mechanism responsible for this behaviour is the existence of local Marangoni stresses near the contact line, acting outwards on both sides of the droplet. As was explained above, a similar mechanism is also present in the case of self-rewetting fluids when the position of the minimum surface tension is located inside the droplet resulting in thermally induced "superspreading".

dx.doi.org/10.1021/la5002682 | *Langmuir* 2014, 30, 4310–4321

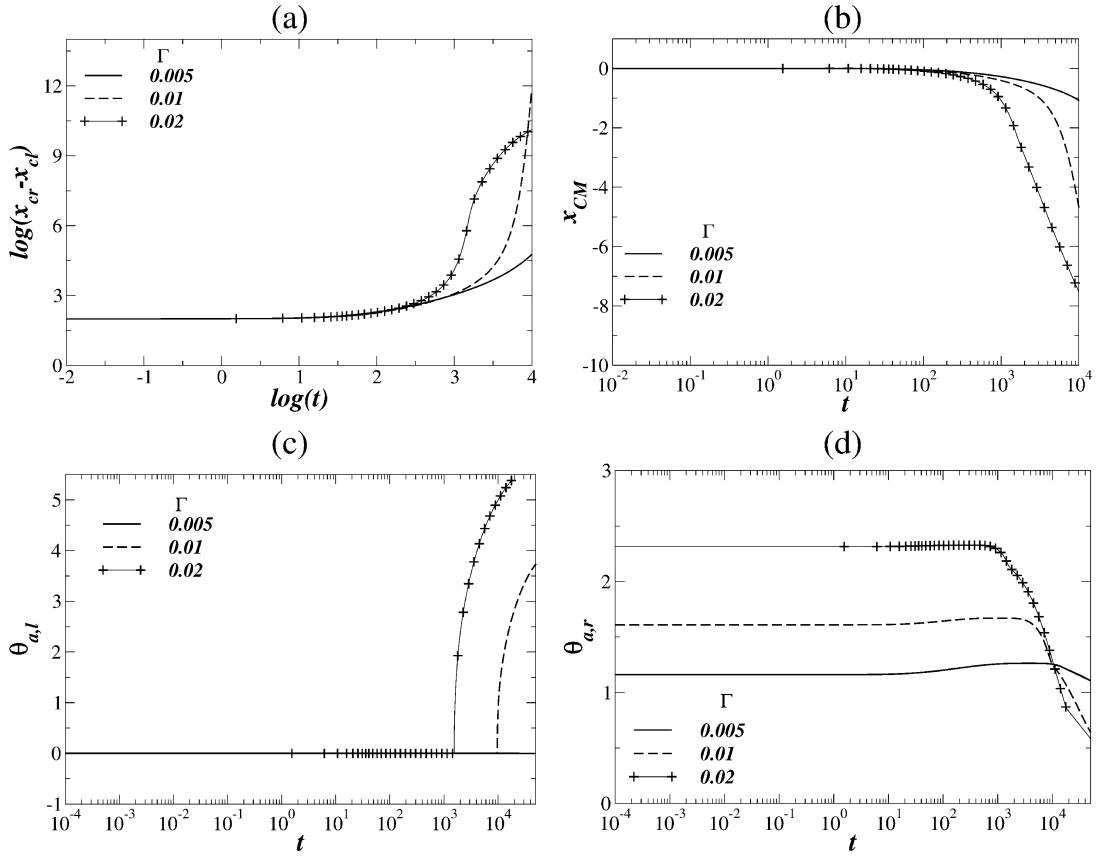

Figure 9. Evolution of the (a) extent of spreading, (b) the position of the center of mass of the droplet, and equilibrium contact angles (c) $\theta_{a,l}$, (d) $\theta_{a,r}$ for different values of Γ. The rest of the parameter values are the same as those used to generate Figure 8.

Varying θ_a. As was mentioned above, in order for the assumption of constant θ_a to be valid, the surface tensions of the substrate and liquids must have an identical dependence on temperature ($C_{lg,1} = C_{ls1} = C_{sg1}$ and $C_{lg,2} = C_{ls2} = C_{sg2}$); it is evident that this assumption is rather restrictive. Here, we discuss the results generated for a dynamic contact angle that varies dynamically through the change of substrate wettability driven by wall-heating. In eq 12, we set $C_{ls,2} = C_{sg,2} = 0$ for the remainder of this paper; this corresponds to a linear dependence of σ_{ls} and σ_{sg} on T_s. Thus, we focus only on the effects that can be attributed to the nonlinear dependence of the gas−liquid interfacial tension on temperature.

In Figure 5, we show the dependence of the spreading dynamics on $C_{lg,1}$ with the rest of the parameters remaining fixed. For cases wherein the minimum in the σ_{lg}−x curve is located to the left of the symmetry plane, and outside of the initial drop profile, $x = 0$, characterized by $C_{lg,1} = -0.5$, the drop spreads in the direction of highest tension, toward the right domain boundary, and behaves similarly to the case of an ordinary fluid. This is driven by Marangoni stresses which act in the same direction across the liquid−gas interface.The drop is deformed in the direction of spreading, and the location of the maximal thickness shifts from the flow origin toward the right contact line, x_{cr}. The left contact line, x_{cl}, moves toward the left at early times, but remains essentially pinned thereafter.

As $C_{lg,1}$ becomes progressively positive, and the location of the minimal σ_{lg} moves to the right of $x = 0$, the direction of spreading is reversed in comparison to the $C_{lg,1} = -0.5$ case. Here, the spreading proceeds with x_{cl} advancing toward the left domain boundary, which coincides with the largest value of σ_{lg}, and x_{cr} moves at a much slower rate also to the left. The spreading speed is also considerably larger than the $C_{lg,1} = -0.5$ case with high power-law exponents, and is accompanied by the formation of thickened ridges at the left contact line, x_{cl}, as shown in Figures 5 and 6. These features are qualitatively similar to those observed in the case of constant equilibrium contact angle, θ_a, and the enhancement of spreading rate shares the same mechanism as discussed in the previous section.

Interestingly, we note that the spreading in the $C_{lg,1} = -0.1$ case takes place in the opposite direction from the one shown for constant θ_a (compare Figures 2a and 5b). Moreover, we notice that the spreading in the $C_{lg,1} = 0$ case, for which the location of the σ_{lg}−x minimum coincides with $x = 0$, is markedly asymmetric; this is also in contrast to the analogous constant θ_a case, shown in Figure 2b, for which the spreading is symmetric. These two cases illustrate the important role of accounting for local variations of θ_a in modeling the spreading dynamics.

In Figure 7, we plot the temporal variation of the dynamic and equilibrium contact angles at the left and right contact lines for different values of $C_{lg,1}$. For $C_{lg,1} = -0.5$, where the thermocapillary stresses drive spreading toward the highest σ_{lg} at the right boundary, the spreading is aided by $\theta_r - \theta_{a,r}$, which remains positive for the time duration considered. For x_{cl}, which becomes the receding contact line at intermediate times, the equilibrium contact angle $\theta_{a,l}$ is zero-valued for the entire computation, and $\theta_l - \theta_{a,l}$ also remains positive. This is because σ_{lg} achieves a low value at the left of $x = 0$ (see Figure 1), which makes $\theta_{a,l}$ negative, as can be seen from eq 18; this is then set to zero. The positive $\theta_l - \theta_{a,l}$ however, provides no wettability driving force for spreading and x_{cl} becomes essentially pinned.

dx.doi.org/10.1021/la5002682 | Langmuir 2014, 30, 4310−4321

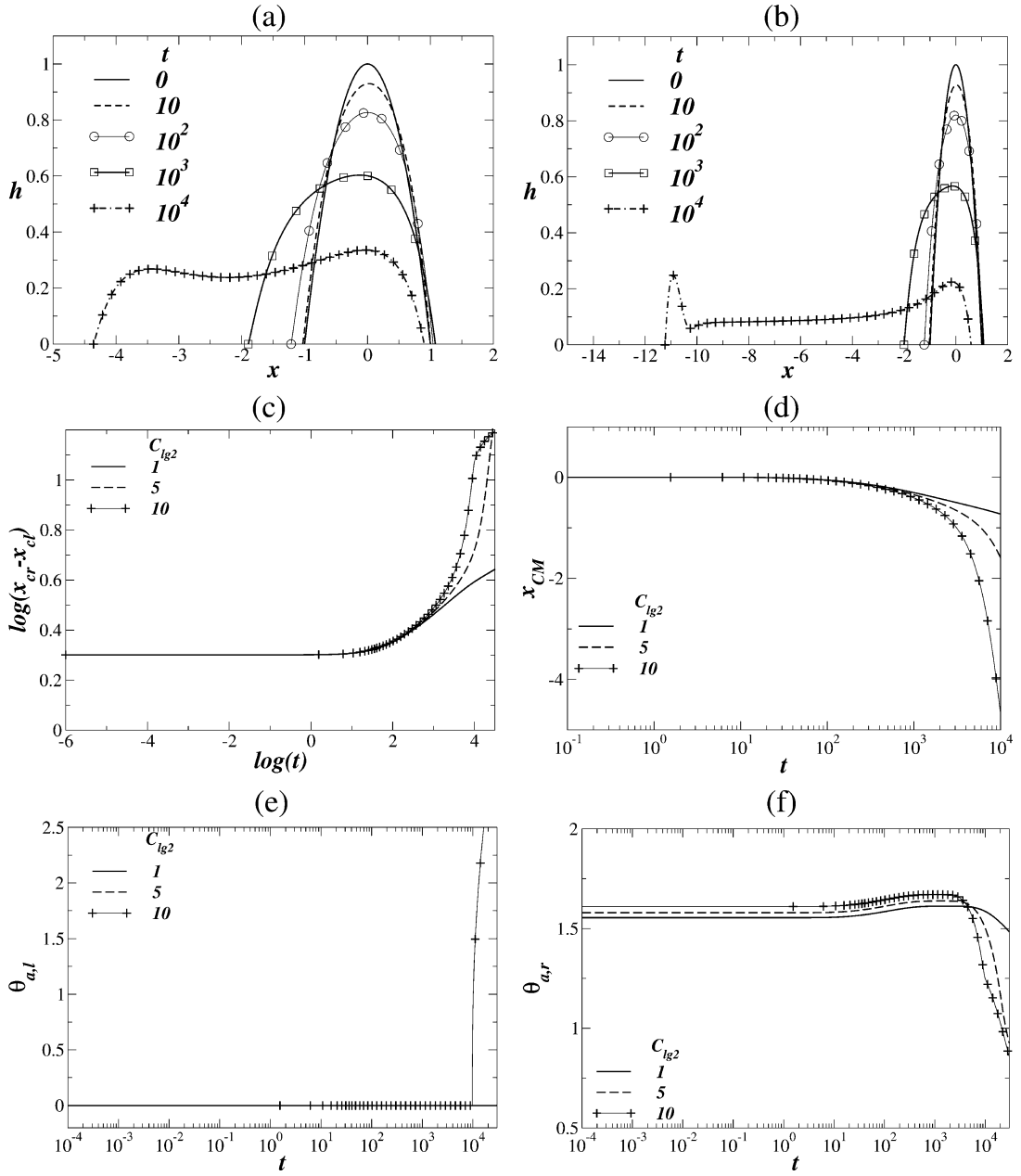

Figure 10. Time snapshots of the drop profile for (a) $C_{lg,2} = 5$ and (b) $C_{lg,2} = 10$. Evolution of the (c) extent of spreading, (d) the position of the center of mass of the droplet, and equilibrium contact angles (e) $\theta_{a,l}$, (f) $\theta_{a,r}$ for different values of $C_{lg,2}$. The rest of the parameter values are $\varepsilon = 0.1$, Ca = 100, $C_{ls1} = C_{sg1} = 1$, $C_{lg,1} = -0.1$, $C_{sg2} = C_{ls2} = 0$, $k = 10^{-3}$, $m = 3$, Bo = 0.5, $\Gamma = 0.01$, $\delta_{ls} = 1$, and $S = -0.001$. The locations of the minimum surface tension in panels (a) and (b) are -1 and -0.5, respectively.

As $C_{lg,1}$ increases, thermocapillarity spreads the drop toward the left, as discussed above. For $C_{lg,1} = -0.1$ the position of minimum σ_{lg} is located inside the droplet and closer to the left edge, and naively, we would expect that the drop would move to the right; this is true in the case of constant θ_a (see Figure 2a). Instead, we find that the droplet spreads in the opposite direction. This effect is due to the fact that the surface energy of the substrate is affected by the imposed temperature gradient. The surface energy on the left side of the droplet is lower which facilitates the initial spreading in this direction that is later enhanced by the presence of Marangoni stresses stretching the droplet. As shown in Figure 7, the advancing contact line for $C_{lg,1} \geq -0.1$ is x_{cl} for which $\theta_l - \theta_{a,l}$ is positive, which accelerates its spreading. This, then, leads to an increase in θ_l for times above $t \sim 10^3$, which coincides with the formation of the thickened ridge at x_{cl}, and further increases $\theta_l - \theta_{a,l}$, accelerating the spreading rate. For x_{cr}, which becomes the receding contact line at intermediate times, the difference $\theta_r - \theta_{a,r}$ becomes negative which aids the motion of x_{cr} toward the left. The equilibrium angle $\theta_{a,r}$ remains positive, since σ_{lg} is relatively large near the right boundary due to the quadratic dependence of σ_{lg} on T_s while σ_{sg} and σ_{ls}, which depend linearly on T_s, attain their lowest values at this hot boundary. Note that the value of $\theta_{a,r}$ in this varying $-\theta_a$ case exceeds that used to generate the results in the previous section, where θ_a was held constant, until the very latest stages of the spreading. The negative $\theta_r - \theta_{a,r}$ difference, however, is not as large as that associated with x_{cl}; consequently, the motion of the right contact line is considerably slower.

dx.doi.org/10.1021/la5002682 | Langmuir 2014, 30, 4310−4321

Next, we examine the dependence of the dynamics on the temperature gradient, Γ, in the variable θ_a case. We show in Figure 8 the drop spreading profiles for different values of Γ with all other parameters remaining constant. For the lowest Γ values studied, the effects associated with the quadratic dependence of σ_{lg} on T_s are small, and the extent of spreading is rather modest even at relatively late times. With increasing Γ, however, these effects become accentuated leading to the "superspreading"-like behaviour discussed above, as shown in Figures 8 and 9. For Γ = 0.02, the temperature gradient is sufficiently large so as to drive the formation of very large ridges at the left contact line, x_{cl}, which contains the majority of the fluid in the drop, and a trailing thin film. We also note that there is a non-monotonic dependence of the spreading rate on the applied temperature gradient, Γ. For high values of Γ, the surface energy of the substrate is affected significantly, and as the droplet spreads to the left the contact line experiences an increasingly hydrophobic surface inhibiting the spreading process (see Figure 9c). The effect of a temperature-varying substrate wettability was also discussed in Karapetsas et al.[20] where a similar behaviour was reported even for liquids with a linear dependence on surface tension.

We also explore the effect of varying $C_{lg,2}$ on the dynamics while keeping the rest of the parameters fixed; this parameter controls the quadratic dependence of σ_{lg} on T_s. Inspection of Figure 10 reveals that increasing the value of $C_{lg,2}$ has a similar effect to raising Γ: it gives rise to lower surface tension minima and larger thermocapillary stresses that drive rapid, "superspreading"-type behavior.

Finally, the parameter $C_{lg,2}$ can also be used to control whether the liquid−air interface exhibits a minimum or a maximum surface tension at a given temperature. As mentioned above, in the case of self-rewetting fluids, this parameter is positive, whereas for a system that exhibits a maximum surface tension this parameter is negative. Systems with the latter behavior have been reported in the literature.[47] We performed a set of simulations for $C_{lg,2} = -10$ and for such values of $C_{lg,1}$ that the position of maximum σ_{lg} resides inside the droplet (e.g., $C_{lg,1} = -0.1, 0, 0.1$) which are not presented here for conciseness. We found that in this case the induced Marangoni stresses drive flow toward the position of maximum surface tension inhibiting the spreading process. The spreading exponent for the cases that we have investigated was found to be much lower than in the case of self-rewetting fluids discussed above.

CONCLUSIONS

We have carried out an investigation of thermocapillary-driven droplet spreading on nonuniformly heated substrates; the effect of a nonlinear dependence of the surface tension on temperature was the focus of the present work. We have used the lubrication approximation to derive an evolution equation for the interface that accounts for capillary and thermocapillary forces. The energy equation within the drop was assumed to be dominated by conduction, and heat transfer from the interface was neglected. The potential singularity at the contact line was relieved via use of a Navier slip condition at the wall and a Cox-Voinov-type relation at the moving contact line. The equilibrium contact angles were allowed to depend on the substrate temperature through their dependence on the gas−liquid, liquid−solid, and gas−solid interfacial tensions.

Numerical solutions of the evolution equation for the interface were obtained for various gas−liquid surface tension−temperature curves, which exhibited a surface tension minimum over the temperature range considered; these included cases wherein the location of this minimum was initially inside the drop, and others in which the minimum was located to either side of the drop. In the latter case, thermocapillary stresses induce droplet spreading away from the surface tension minimum, causing both contact lines to move in the same direction. In the former cases, however, our results demonstrate that thermocapillary stresses drive flow away from the surface tension minimum within the droplet, causing the contact lines to move in opposite directions. This, in turn, accelerates the spreading significantly to the extent that the spreading characteristics, in terms of power-law exponents and interfacial shapes, resemble those that accompany surfactant-driven "superspreading" of droplets on hydrophobic substrates. In particular, the power-law exponents approach a value of unity during the spreading, and the latter is accompanied by the formation of pronounced ridges at the advancing contact lines. Fluids that are associated with either a linear dependence of the surface tension on temperature, or a maximum in the surface tension-temperature, curve do not exhibit this type of behavior.

AUTHOR INFORMATION

Corresponding Author

*E-mail: gkarapetsas@gmail.com.

Notes

The authors declare no competing financial interest.

REFERENCES

(1) Thampi, S. P.; Govindarajan, R. Minimum energy shapes of one-side-pinned static drops on inclined surfaces. *Phys. Rev. E* **2011**, *84*, 046304.

(2) de Gennes, P. G. Wetting: statics and dynamics. *Rev. Mod. Phys.* **1985**, *57*, 827.

(3) Bonn, D.; Eggers, J.; Indekeu, J.; Meunier, J.; Rolley, E. Wetting and spreading. *Rev. Mod. Phys.* **2009**, *81*, 739−805.

(4) Bouasse, H. *Capillarite: phenomenes superficiels*; Librairie Delgrave: Paris, 1924.

(5) Brzoska, J. B.; Brochard-Wyart, F.; Rondelez, F. Motions of droplets on hydrophobic model surfaces induced by thermal gradients. *Langmuir* **1993**, *9*, 2220−2224.

(6) Chen, J. Z.; Troian, S. M.; Darhuber, A. A.; Wagner, S. Effect of contact angle hysteresis on thermocapillary droplet actuation. *J. Appl. Phys.* **2005**, *97*, 014906.

(7) Brochard, F. Motions of droplets on solid surfaces induced by chemical or thermal gradients. *Langmuir* **1989**, *5*, 432−438.

(8) Ford, M. L.; Nadim, A. Thermocapillary migration of an attached drop on a solid surface. *Phys. Fluids* **1994**, *6*, 3183−3185.

(9) Ehrhard, P.; Davis, S. H. Non-isothermal spreading of liquid drops on horizontal plates. *J. Fluid Mech.* **1991**, *229*, 365−388.

(10) Dunn, G. J.; Duffy, B. R.; Wilson, S. K.; Holland, D. Quasi-steady spreading of a thin ridge of fluid with temperature-dependent surface tension on a heated or cooled substrate. *Quarterly Journal of Mechanics and Applied Mathematics* **2009**, *62*, 365−402.

(11) Anderson, D. M.; Davis, S. H. The spreading of volatile liquid droplets on heated surfaces. *Phys. Fluids* **1995**, *7*, 248.

(12) Karapetsas, G.; Matar, O. K.; Valluri, P.; Sefiane, K. Convective rolls and hydrothermal waves in evaporating sessile drops. *Langmuir* **2012**, *28*, 11433−11439.

(13) Chen, J.-C.; Kuo, C.-W.; Neitzel, G. Numerical simulation of thermocapillary nonwetting. *Int. J. Heat Mass Transfer* **2006**, *49*, 4567−4576.

(14) Nguyen, H.-B.; Chen, J.-C. Numerical study of a droplet migration induced by combined thermocapillary-buoyancy convection. *Phys. Fluids* **2010**, *22*, 122101−122101−9.

(15) Smith, M. K. Thermocapillary migration of a two-dimensional liquid droplet on a solid surface. *J. Fluid Mech.* **1995**, *294*, 209−230.

(16) Gomba, J. M.; Homsy, G. M. Regimes of thermocapillary migration of droplets under partial wetting conditions. *J. Fluid Mech.* **2010**, *647*, 125.
(17) Pratap, V.; Moumen, N.; Subramanian, R. S. Thermocapillary motion of a liquid drop on a horizontal solid surface. *Langmuir* **2008**, *24*, 5185−5193.
(18) Daniel, S.; Chaudhury, M. K.; Chen, J. C. Fast drop movements resulting from the phase change on a gradient surface. *Science* **2001**, *291*, 633−636.
(19) Wasan, D. T.; Nikolov, A. D.; Brenner, H. Droplets speeding on surfaces. *Science* **2001**, *291*, 605−606.
(20) Karapetsas, G.; Sahu, K. C.; Matar, O. K. Effect of contact line dynamics on the thermocapillary motion of a droplet on an inclined plate. *Langmuir* **2013**, *29*, 8892−8906.
(21) Vochten, R.; Petre, G. Study of heat of reversible adsorption at air-solution interface 2. Experimental determination of heat of reversible adsorption of some alcohols. *J. Colloid Interface Sci.* **1973**, *42*, 320−327.
(22) Petre, G.; Azouni, M. A. Experimental evidence for the minimum of surface tension with temperature at aqueous alcohol solution air interfaces. *J. Colloid Interface Sci.* **1984**, *98*, 261−263.
(23) Legros, J. C.; Limbourg-Fontaine, M. C.; Petre, G. Influence of a surface tension minimum as a function of temperature on the marangoni convection. *Acta Astronautica* **1984**, *11*, 143−147.
(24) Limbourg-Fontaine, M. C.; Petre, G.; Legros, J. C. Thermocapillary movements under at a minimum of surface tension. *Naturwissenschaften* **1986**, *73*, 360−362.
(25) Savino, R.; Cecere, A.; Paola, R. D. Surface tension driven flow in wickless heat pipes with self-rewetting fluids. *Int. J. Heat Fluid Flow* **2009**, *30*, 380−388.
(26) Savino, R.; Cecere, A.; Vaerenbergh, S. V.; Abe, Y.; Pizzirusso, G.; Tzevelecos, W.; Mojahed, M.; Galand, Q. Some experimental progresses in the study of the self-rewetting fluids for the SELENE experiment to be carried in the Thermal Platform 1 hardware. *Acta Astronautica* **2013**, *89*, 179−188.
(27) Oron, A.; Rosenau, P. On a nonlinear thermocapillary effect in thin liquid layers. *J. Fluid Mech.* **1994**, *273*, 361−374.
(28) Slavtchev, S. G.; Miladinova, S. P. Thermocapillary flow in a liquid layer at minimum in surface tension. *Acta Mechanica* **1998**, *127*, 209−224.
(29) Abe, Y.; Iwasaki, A.; Tanaka, K. Microgravity experiments on phase change of self-rewetting fluids. *Ann. N.Y. Acad. Sci.* **2004**, *1027*, 269−285.
(30) Suzuki, K.; Nakano, M.; Itoh, M.Subcooled boiling of aqueous solution of alcohol, 2005
(31) Mcgillis, W. R.; Carey, V. P. On the role of Marangoni effects on the critical heat flux for pool boiling of binary mixtures. *Trans. ASME J. Heat Transfer* **1996**, *118*, 103−109.
(32) Ahmed, S.; Carey, V. P. Effects of surface orientation on the pool boiling heat transfer in water/2-propanol mixtures. *Trans. ASME J. Heat Transfer* **1999**, *121*, 80−88.
(33) Hu, Y.; Liu, T.; Li, X.; Wang, S. Heat transfer enhancement of micro oscillating heat pipes with self-rewetting fluid. *Int. J. Heat Mass Transfer* **2014**, *70*, 496−503.
(34) Karapetsas, G.; Craster, R. V.; Matar, O. K. On surfactant-enhanced spreading and superspreading of liquid drops on solid surfaces. *J. Fluid Mech.* **2011**, *670*, 5−37.
(35) McHale, G.; Brown, C. V.; Sampara, N. Voltage-induced spreading and superspreading of liquids. *Nat. Commun.* **2013**, *4*, 1605.
(36) Hu, H.; Larson, R. G. Analysis of the microfluid flow in an evaporating sessile droplet. *Langmuir* **2005**, *21*, 3963−3971.
(37) Hu, H.; Larson, R. G. Analysis of the effects of Marangoni stresses on the microflow in an evaporating sessile droplet. *Langmuir* **2005**, *21*, 3972−3980.
(38) Cazabat, A. M.; Heslot, F.; Troian, S. M.; Carles, P. Fingering instability of thin spreading films driven by temperature gradients. *Nature* **1990**, *346*, 824.
(39) Navier, C. L. M. H. Memoire sur les lois du mouvement des fluides. *Acad. R. Sci. Inst. Fr.* **1823**, *6*, 389−440.
(40) Tanner, L. H. The spreading of silicone oil drops on horizontal surfaces. *J. Phys. D: Appl. Phys.* **1979**, *12*, 1473−84.
(41) Haley, P. J.; Miksis, M. J. The effect of the contact line on droplet spreading. *J. Fluid Mech.* **1991**, *223*, 57−81.
(42) Benintendi, S. W.; Smith, M. K. The spreading of a non-isothermal liquid droplet. *Phys. Fluids* **1999**, *11*, 982−989.
(43) K. Y. Chan, A. B. Surfactant-assisted spreading of a liquid drop on a smooth solid surface. *J. Colloid Interface Sci.* **2005**, *287*, 233−248.
(44) Ehrhard, P. Experiments on isothermal and non-isothermal spreading. *J. Fluid Mech.* **1993**, *257*, 463−483.
(45) Savva, N.; Kalliadasis, S. Two-dimensional droplet spreading over topographical substrates. *Phys. Fluids* **2009**, *21*, 092102.
(46) Qian, T.; Wang, X.-P.; Sheng, P. Molecular scale contact line hydrodynamics of immiscible flows. *Phys. Rev. E* **2003**, *68*, 016306.
(47) Villers, D.; Platten, J. K. Temperature dependence of the interfacial tension between water and long-chain alcohols. *J. Phys. Chem.* **1988**, *92*, 4023−4024.